Nonlinear Model Predictive Control for the Stabilization of a Wheeled Unmanned Aerial Vehicle on a Pipe

Suping Zhao[1,2], Fabio Ruggiero[2], Giuseppe Andrea Fontanelli[2], Vincenzo Lippiello[2], Zhanxia Zhu[1], Bruno Siciliano[2]

***Abstract*—This letter addresses the task of stabilizing a wheeled unmanned aerial vehicle on a pipe, which is an emerging application in oil and gas facilities for nondestructive measurements. After the derivation of the dynamic model of the system, a discrete-time nonlinear model predictive controller is designed over a finite horizon. The analysis of the asymptotic stability of the designed controller is carried out. Numerical tests show the performance and the robustness of the proposed solution.**

***Index Terms*—Nonlinear model predictive control, wheeled unmanned aerial vehicle, nondestructive testing**

I. INTRODUCTION

THE SPARC multi-annual roadmap, released in its final version in December 2016, considers the inspection and maintenance as a pillar domain in which robots can provide significant advantages over current methods. Within this background, nondestructive contact measurements are widely adopted in industrial scenarios such as oil and gas facilities. In particular, this work is rooted in the HYFLIERS project [www.oulu.fi/hyfliers] whose aim is to study and develop solutions to perform inspection measurements with reduced exposure to risks and costs. To this end, a hybrid aerial-ground robot with a hyper-redundant lightweight robotic arm, equipped with an inspection sensor, will be developed within the project, together with supporting services for efficient and safe navigation in a complex and safety-critical environment.

The hybrid aerial-ground robot is mainly made up by a wheeled unmanned aerial vehicle (WUAV) landing on a horizontal pipe to perform the required measurements. It is supposed to have enough space for approaching and moving around. The wheels are necessary to agilely navigate on the pipe, thus reducing the power consumption for the case of using only an aerial vehicle. As better specified in the attached technical report, two Mecanum wheels are put in the front of the vehicle to orientate and navigate on the pipe, while two Omni-wheels are put in the back for the orientation on the pipe. Since the landing of the WUAV on the pipe may be inaccurate (not exactly on the top), and because during the navigation on the pipe some disturbances may affect the motion, it is necessary to continually stabilize the vehicle against gravity, avoiding the slippage of the wheels. To this end, once the WUAV has landed on the pipe, its propellers can be tilted providing a lateral thrust that can help in case the torques of the wheels saturate. The concept of the described WUAV is sketched in Fig. 1.

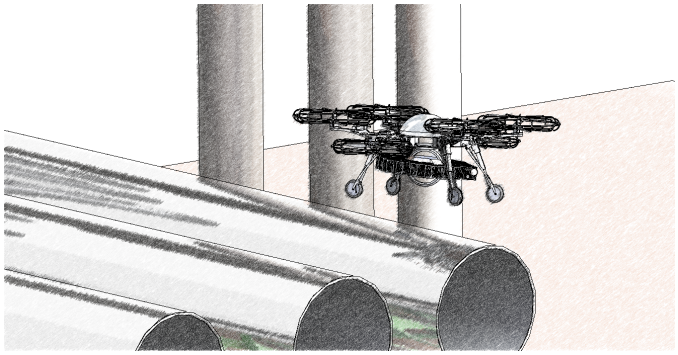

Fig. 1. Concept of the WUAV device employed within the HYFLIERS project for nondestructive tests within oil and gas facilities.

Therefore, this letter investigates the simpler yet interesting task of stabilizing a planar WUAV on a pipe through a discrete-time nonlinear model predictive control (NMPC). The NMPC controller is chosen to handle the slipping constraints explicitly and the saturation of the actuators, robustifying the control action. Closed-loop asymptotic stability is guaranteed as well. Next section revises the current state of the art, having the outcome that the novelty of this letter is doubtless the application, whose solution may be relevant within nondestructive measurements in oil and gas facilities. Section III develops the dynamic model of the planar WUAV on the pipe through the Newton-Euler approach, considering as inputs the lateral thrust (provided by the tilted propellers) and the torques of the wheels. Afterwards, the constraints necessary to stabilize the WUAV on the pipe are adequately derived. The discrete-time optimal control problem and the NMPC are developed in Section IV. The performance of the proposed approach is tested in Section V with a critical discussion about the carried out results. Section VI concludes the letter. The technical report, attached as multimedia material to this letter, illustrates the devices under construction, their characteristics, and their weakness. Besides, the first experiment on a device with only

Manuscript received: February 24, 2019; Revised June 1, 2019; Accepted July 8, 2019.

This paper was recommended for publication by Editor Jonathan Roberts upon evaluation of the Associate Editor and Reviewers comments.

*The research leading to these results has been supported by the HYFLIERS project (Horizon 2020 Grant Agreement No. 779411).

[1]National Key Laboratory of Aerospace Flight Dynamics, Northwestern Polytechnical University, 127 Youyi West Road, Xi'an, 710072, China suping36@mail.nwpu.edu.cn, zhuzhanxia@nwpu.edu.cn

[2]CREATE Consortium and PRISMA Lab, Department of Engineering and Information Technology, University of Naples Federico II, Via Claudio 21, Naples, 80125, Italy {fabio.ruggiero, giuseppeandrea.fontanelli, vincenzo.lippiello, bruno.siciliano}@unina.it

Digital Object Identifier (DOI): see top of this page.

wheels, without the propellers, is shown.

II. STATE OF THE ART

Nondestructive measurement tests (NDT) in refineries are currently performed by human operators climbing huge and costly scaffolding. Several robotic commercial solutions are currently (or are ready-to-be) available like the APPELLIX drone [www.apellix.com], the Texo Drone Survey and Inspection platform [www.texodroneservices.co.uk/blog/56], and the Ronik Inspectioneering UT device [www.inspectioneering.eu]. The listed devices are drones equipped with a stick, or a telescopic arm, at whose tip is mounted an ultrasonic thickness sensor. As highlighted in several research works, the contact between the stick and the surface may destabilize the robot, because the contact arises a torque at the center of mass of the drone. Several solutions address such a problem. The impacts destabilizing the aerial device are addressed in [1] by combining mechanics, with the use of active and passive joints, and control strategy. The impacts may also be absorbed through a passive vacuum-cup technology as in [2]. The problem of carrying out large forces in contact with the environment with an underactuated drone is instead investigated in [3] through the use of LQR-optimized state feedback on the roll and yaw angle. In case the inspections measurements are performed in a crowded and narrow environment, and the drone is too bulky to stay close to the surface to be inspected, a long reach aerial manipulator can be employed [4].

The solution proposed within the HYFLIERS project for NDT is innovative. The hybrid aerial-ground robot is efficient since it does not require to fly during all the inspection operation, but it can land and navigate on pipes. The stabilization of a hybrid aerial-ground robot on a pipe is indeed a new problem. To the authors' knowledge, a thorough search of the relevant literature reveals that it does not exist any paper addressing a task similar to the one tackled by this letter. The most similar applications may be found in those employing climbing [5] and perching robots [6]. The former can climb on the surface of objects with different surface roughness, and the latter can perch on the surface of an object to eventually perform some manipulation tasks. For both categories of robots, the research usually focuses on the adhesive mechanism, mainly including the magnetic adhesion [7], the pneumatic adhesion [8], the mechanical adhesion [9], the electrostatic adhesion [10], and the chemical adhesion [11]. As the aim of this work, the crucial element in climbing and perching robots is the stability of robotic systems on the surface of a telegraph pole [12], [13] or a wall [14], [15]. Both the mechanical structure and the employed control methods are critical for the stability of the system. A proportional-integral-derivative (PID) controller is built in [12] to govern the motion of a robotic system on a pipe, but the wheels of the robotic system are assumed not to slip. A PID-based methodology is also employed in [14] to generate desired pressure between a wheeled robotic system and a non-smooth vertical wall and a horizontal ceiling. A proportional-derivative (PD) controller is instead built in [13] to achieve high-speed climbing of a quadrupedal robot on a wooden telegraph pole. A PD control method is also employed in [15] to follow the desired motion of a hexapedal robot on brick- or stucco-walls. Other methods include the autonomous control [16] of the motion of a robotic system with "mother-child"-structure on thin surfaces and the decentralized parallel control [17] of a six-legged wall climbing robot with high payloads.

Other approaches solving such a kind of task make use of the NMPC as in [18] for an elastic tool interaction of the drone with the ceiling. In general, in the last decades, MPC and NMPC dominate the process industry for a large variety of applications [19]. Critical discussions, theoretical advantages, and quantitative results of using MPC and NMPC over the classical methodologies, like a PID-based controller, can be found in [20], [21], [22, Section 1.3]. Therefore, the use of NMPC over the classical control approaches allow the possibility to explicitly include the slipping conditions and saturation of the actuators within the control design. The NMPC can be categorized into continuous-time [23] and discrete-time [24] settings. The discrete-time setting, employed in this letter, is preferred due to the simplicity of notation, the conceptual formulation, and the intrinsic discrete nature of the elaboration systems. Various approaches are then investigated to guarantee the stability of a discrete-time NMPC, and they are reviewed in [24]: the terminal state cost penalty [25]–[28], and the terminal inequality constraint [25], [28], [29] are critical instruments in the design of the controller. Besides, the linearization of the nonlinear system is addressed in [26]: based on the stability of the locally linearized system, the exponential stability at the equilibrium is guaranteed. A similar approach with an infinite time horizon is tackled in [27]. In [30], the optimization problem with an infinite time horizon is reduced to a convex optimization problem with linear inequality constraints, and the uniform asymptotic stability is proved through the Lyapunov approach. The NMPC with a finite time horizon is also employed in [29] to control a multiplicative noise stochastic system, where the input delay is considered, and the stability is guaranteed by introducing two terminal inequalities.

III. DYNAMIC MODEL AND STABILIZATION CONSTRAINTS

A. Dynamic model of the WUAV system on a pipe

Some simplifications are made to derive the dynamic model of the system briefly described in the introduction. i) The wheels are in a fixed position, and they can move transversely to the pipe to constrain the motion of the WUAV only around the circumference. ii) The propellers are in a fixed position such as the combined effect of the center of mass of the WUAV is always parallel to the tangent to the pipe. iii) The wheels and the pipe are rigid and a Coulomb friction model is assumed, while the rolling friction is negligible. iv) The wheels do not slip on the pipe. v) The inertia of the wheels and the propellers are negligible compared to the inertia of the WUAV rotation around the center of the pipe.

With the above assumptions, the resulting system is sketched in Fig. 2. Since the system is symmetric to the vertical plane cutting the WUAV at its center of mass, a two-dimensional (2-D) representation can be employed to further

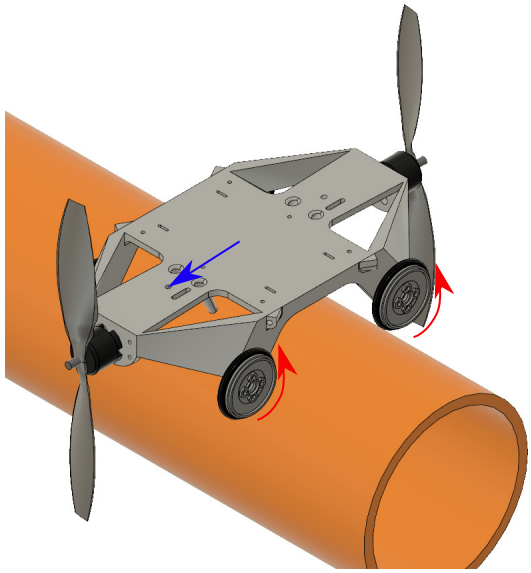

Fig. 2. Three-dimensional sketch of the WUAV system on a pipe. In red, the actuation torques on the wheels. In blue, the effect of the propeller effects on the center of mass of the WUAV.

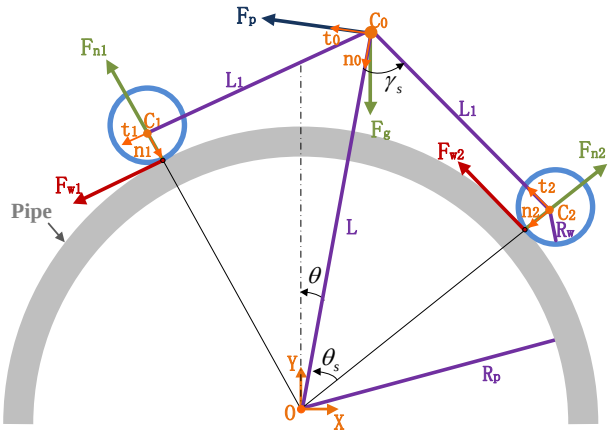

Fig. 3. 2-D sketch of the WUAV system on a pipe, with the illustration of the symbols employed to derive the dynamic model of the WUAV and its constraints.

simplify the derivation of the dynamic model. Therefore, with reference to Fig. 3, the origin O of the inertial reference frame Σ_B is put in the center of the pipe, while the Y-axis is directed along the gravity direction, and the X-axis is directed along the radius of the pipe and parallel to the ground. Three coordinate frames, Σ_i, with $i = 0, 1, 2$, are instead attached to the WUAV. The frame Σ_0 is placed at the center of mass of the WUAV, with $\boldsymbol{n}_o \in \mathbb{R}^2$ the unit vector always directed towards the center of the pipe, and $\boldsymbol{t}_o \in \mathbb{R}^2$ the unit vector perpendicular to $\boldsymbol{n}_0$ and parallel to the tangent to the pipe. The frames Σ_1 and Σ_2 are placed at the center of the wheels, with $\boldsymbol{n}_1 \in \mathbb{R}^2$ and $\boldsymbol{n}_2 \in \mathbb{R}^2$ the unit vectors always directed towards the center of the pipe, and $\boldsymbol{t}_1 \in \mathbb{R}^2$ and $\boldsymbol{t}_2 \in \mathbb{R}^2$ the unit vectors perpendicular to $\boldsymbol{n}_1$ and $\boldsymbol{n}_2$, respectively, and parallel to the tangent to the pipe. The expression of the mentioned vectors in Σ_B are

$$\boldsymbol{t}_0 = \begin{bmatrix} -\cos(\theta) & -\sin(\theta) \end{bmatrix}^T, \tag{1a}$$
$$\boldsymbol{n}_0 = \begin{bmatrix} \sin(\theta) & -\cos(\theta) \end{bmatrix}^T, \tag{1b}$$
$$\boldsymbol{t}_1 = \begin{bmatrix} -\cos(\theta_s + \theta) & -\sin(\theta_s + \theta) \end{bmatrix}^T, \tag{1c}$$
$$\boldsymbol{n}_1 = \begin{bmatrix} \sin(\theta_s + \theta) & -\cos(\theta_s + \theta) \end{bmatrix}^T, \tag{1d}$$
$$\boldsymbol{t}_2 = \begin{bmatrix} -\cos(\theta_s - \theta) & \sin(\theta_s - \theta) \end{bmatrix}^T, \tag{1e}$$
$$\boldsymbol{n}_2 = \begin{bmatrix} -\sin(\theta_s - \theta) & -\cos(\theta_s - \theta) \end{bmatrix}^T. \tag{1f}$$

The inputs to the system are the lateral thrust $F_p \in \mathbb{R}$ created by the propellers, and the torques of the wheels $\tau_{w1}, \tau_{w2} \in \mathbb{R}$. The following vectors can be thus defined in Σ_B

$$\boldsymbol{F}_p = \begin{bmatrix} -F_p \cos(\theta) & -F_p \sin(\theta) \end{bmatrix}^T, \tag{2a}$$
$$\boldsymbol{F}_{w1} = \begin{bmatrix} -F_{w1} \cos(\theta_s + \theta) & -F_{w1} \sin(\theta_s + \theta) \end{bmatrix}^T, \tag{2b}$$
$$\boldsymbol{F}_{w2} = \begin{bmatrix} -F_{w2} \cos(\theta_s - \theta) & F_{w2} \sin(\theta_s - \theta) \end{bmatrix}^T, \tag{2c}$$

with $F_p = \|\boldsymbol{F}_p\|$, $F_{w1} = \|\boldsymbol{F}_{w1}\| = \tau_{w1}/R_w$, $F_{w2} = \|\boldsymbol{F}_{w2}\| = \tau_{w2}/R_w$, and $R_w \in \mathbb{R}^+$ the radius of both wheels. Throughout the letter, the norms are Euclidean.

Finally, let $L \in \mathbb{R}^+$ be the distance between the center of the pipe and the center of mass of the WUAV, $\theta \in \mathbb{R}$ the angle of the WUAV with respect to the Y-axis, $\gamma_s \in \mathbb{R}$ and $\theta_s \in \mathbb{R}$ two angles depending on the geometry of the device and the pipe, and $R_p \in \mathbb{R}^+$ the radius of the pipe. Based on the Newton-Euler theory, the dynamic model of the system is formulated as

$$\ddot{\theta} = \frac{1}{mL} \left[mg \sin(\theta) + F_p + \frac{\cos(\theta_s)}{R_w} (\tau_{w1} + \tau_{w2}) \right], \tag{3}$$

where $m \in \mathbb{R}^+$ is the mass of the WUAV and g is the gravity acceleration.

B. Derivation of the constraints for stabilization

From the walking robots domain, it is useful to import the concept that the resultant of all the forces acting on the robot must remain strictly inside the support polygon to ensure the stability against gravity [31]. Denoting with $\boldsymbol{F}_s = \boldsymbol{F}_g + \boldsymbol{F}_p + \boldsymbol{F}_{w1} + \boldsymbol{F}_{w2}$ the resultant force at the center of mass of the WUAV, expressed in Σ_B with $\boldsymbol{F}_g = \begin{bmatrix} 0 & -mg \end{bmatrix}^T$, these dynamical conditions imply that $\boldsymbol{F}_s$ must lie within the cone of angle $2\gamma_s$. Taking inspiration from the Coulomb's friction law [32], the aforementioned dynamic conditions can be defined through the following constraints expressed in Σ_B

$$\begin{cases} \boldsymbol{F_s}^T \boldsymbol{n_0} > 0, \\ |\boldsymbol{F_s}^T \boldsymbol{t_0}| \leq \tan(\gamma_s) \boldsymbol{F_s}^T \boldsymbol{n_0}. \end{cases} \tag{4}$$

The assumption iv) related to the non-slipping condition of the wheels must be ensured by the controller. Such a condition also ensures that the WUAV does not detach from the pipe while moving. Taking inspiration from [33] for the case of a mobile robot on a flat floor, the procedure to find

the non-slipping constraint is here extended for the case of a wheeled robot on a circular tube. The presence of assumption i) implies that there is not any lateral force acting on the wheels pushing them along the pipe. Therefore, with reference to Fig. 3, the total force acting on each wheel can be decomposed into the tangential force $\boldsymbol{F}_{wi}$, with $i = \{1, 2\}$, and the normal force $\boldsymbol{F}_{ni} \in \mathbb{R}^2$. From the Coulomb model, the no-slipping condition can be expressed as $|F_{wi}| \leq \mu F_{ni}$, where $F_{ni} = \|\boldsymbol{F}_{ni}\|$ and $\mu \in \mathbb{R}^+$ is the static friction coefficient between each wheel and the pipe, whose value depends on the materials at contact. The problem is how to relate F_{Ni} with the other involved forces. Writing the force and moment balance in Σ_B yields

$$\begin{cases} F_{n1}\boldsymbol{n}_1 + F_{n2}\boldsymbol{n}_2 = \boldsymbol{F}_p + \boldsymbol{F}_g, \\ F_{n1}L_1 - F_{n2}L_1 = 0, \end{cases} \tag{5}$$

with $L_1 \in \mathbb{R}^+$ the distance between the center of each wheel and the center of mass of the WUAV. By manipulating (5) with some trigonometric formula, computing F_p in one equation and folding it into the others, it is possible to obtain the following expression for the normal force $F_n = F_{n1} = F_{n2} = \dfrac{mg\cos(\theta)}{2\cos(\theta_s)}$. Hence, replacing the obtained expression into the Coulomb model yields $|F_{wi}| \leq \mu \dfrac{mg\cos(\theta)}{2\cos(\theta_s)}$, and since such a condition is true to maintain the pure rolling assumption, it is possible to write equivalently

$$\begin{cases} |\tau_{w1}| \leq \dfrac{\mu m g R_w cos(\theta)}{2cos(\theta_s)}, \\ |\tau_{w2}| \leq \dfrac{\mu m g R_w cos(\theta)}{2cos(\theta_s)}. \end{cases} \tag{6}$$

IV. DISCRETE-TIME NMPC ALGORITHM

The main idea of the NMPC algorithm is the repetitive solution of an optimal nonlinear control problem (NLP). Given the measured state $\overline{\boldsymbol{x}}_0 := \boldsymbol{x}(k)$, with the state vector $\boldsymbol{x} = \begin{bmatrix} x_1 & x_2 \end{bmatrix}^T = \begin{bmatrix} \theta & \dot{\theta} \end{bmatrix}^T \in \mathbb{R}^2$, at each controller time step $k = 0, T_s, 2T_s, \ldots$, with $T_s \in \mathbb{R}^+$, the discretized version of the dynamic model (3) is employed by the NMPC to predict to future behaviour of the system $\widehat{\boldsymbol{x}}(j)$, with $j = 0, \ldots, N-1$, where $N \geq 2$ denotes the finite prediction horizon. The prediction sequence is useful to determine the optimal control sequence $\overline{\boldsymbol{u}}(0), \overline{\boldsymbol{u}}(1), \ldots, \overline{\boldsymbol{u}}(N-1)$ minimizing the NLP while satisfying the constraints, with the control input vector $\boldsymbol{u} = \begin{bmatrix} u_1 & u_2 & u_3 \end{bmatrix}^T = \begin{bmatrix} F_p & \tau_{w1} & \tau_{w2} \end{bmatrix}^T \in \mathbb{R}^3$. In this case, the control and the prediction horizons are coincident. The peculiarity of the NMPC is to apply only the first element $\boldsymbol{u}(k) := \overline{\boldsymbol{u}}(0) \in \mathbb{R}^3$ of the sequence to the real system. The NLP is repeatedly solved from each new acquired measure.

Then, the NLP at each sampling time k, with initial state $\overline{\boldsymbol{x}}_0$, can be sketched out as

$$\min_{\overline{\boldsymbol{u}}(0)\ldots\overline{\boldsymbol{u}}(N-1)} J = \sum_{j=0}^{N-1} V\left(\widehat{\boldsymbol{x}}(j), \overline{\boldsymbol{u}}(j)\right) + V_N\left(\widehat{\boldsymbol{x}}(N)\right)$$

$$\text{subject to} \tag{7}$$

$$\begin{cases} \widehat{\boldsymbol{x}}(j+1) = \boldsymbol{f}\left(\widehat{\boldsymbol{x}}(j), \overline{\boldsymbol{u}}(j)\right), \\ \boldsymbol{x}_\star \in \mathbb{X}_0 \subseteq \mathbb{X}, \\ \overline{\boldsymbol{u}} \in \mathbb{U}, \\ \boldsymbol{F_s}^T \boldsymbol{n_0} > 0, \\ |\boldsymbol{F_s}^T \boldsymbol{t_0}| \leq \mu_0 \boldsymbol{F_s}^T \boldsymbol{n_0}, \\ |u_2| \leq \dfrac{\mu m g R_w cos(\theta)}{2cos(\theta_s)}, \\ |u_3| \leq \dfrac{\mu m g R_w cos(\theta)}{2cos(\theta_s)}, \end{cases}$$

with the initial state $\widehat{\boldsymbol{x}}(j) = \overline{\boldsymbol{x}}_0$, the discretized version of the dynamic model (3)

$$\boldsymbol{f}(\boldsymbol{x}, \boldsymbol{u}) = \begin{bmatrix} x_1 + T_s x_2 \\ x_2 + T_s\left(\frac{g\sin(x_1)}{L} + \frac{u_1}{mL} + \frac{(u_2+u_3)\cos(\theta_s)}{mLR_w}\right) \end{bmatrix}, \tag{8}$$

the cost function to minimize $V(\widehat{\boldsymbol{x}}(j), \overline{\boldsymbol{u}}(j)) = (\widehat{\boldsymbol{x}}(j) - \boldsymbol{x}_\star)^T \boldsymbol{Q} (\widehat{\boldsymbol{x}}(j) - \boldsymbol{x}_\star) + (\overline{\boldsymbol{u}}(j) - \boldsymbol{u}_\star)^T \boldsymbol{R} (\overline{\boldsymbol{u}}(j) - \boldsymbol{u}_\star)$, the positive definite matrices $\boldsymbol{Q} \in \mathbb{R}^{2\times 2}$ and $\boldsymbol{R} \in \mathbb{R}^{3\times 3}$, the desired equilibrium point of the system (3) $\boldsymbol{x}_\star = \begin{bmatrix} 0 & 0 \end{bmatrix}^T$, and the reference control input $\boldsymbol{u}_\star = \begin{bmatrix} 0 & 0 & 0 \end{bmatrix}^T$. Finally, let $\mathbb{X} \subseteq \mathbb{R}^2$ and $\mathbb{U} \subseteq R^3$ denote the compact sets to impose some bounds on the state and the control inputs, respectively. Moreover, the terminal cost $V_N\left(\widehat{\boldsymbol{x}}(N)\right)$ is employed to penalize the final state of the finite horizon, while the terminal region $\mathbb{X}_0$ is employed to guarantee that the final state of the finite horizon is within a neighbourhood of the reference point.

Both $V_N\left(\widehat{\boldsymbol{x}}(N)\right)$ and $\mathbb{X}_0$ are employed to guarantee the asymptotic stability of the closed loop, as addressed in [24, Theorem 5.13] as follows.

Theorem 1: Consider the NMPC algorithm with discrete-time optimal control problem (7), together with sampling time period T_s and finite time horizon N. If the following assumptions are satisfied, the closed-loop system $\boldsymbol{x}(k+1) = \boldsymbol{f}(\boldsymbol{x}(k), \boldsymbol{u}(k))$ with NMPC feedback law $\boldsymbol{u}(k)$ is asymptotically stable.

- **A1.** The cost function $V\left(\widehat{\boldsymbol{x}}(j), \overline{\boldsymbol{u}}(j)\right)$ and the optimal value function $F(k) := \inf_{\overline{\boldsymbol{u}}(0),\ldots,\overline{\boldsymbol{u}}(N)} J(k)$, must obey the inequalities $V\left(\widehat{\boldsymbol{x}}(j), \overline{\boldsymbol{u}}(j)\right) \geq \alpha_3(\|\boldsymbol{x} - \boldsymbol{x}_\star\|)$ and $\alpha_1(\|\boldsymbol{x} - \boldsymbol{x}_\star\|) \leq F(k) \leq \alpha_2(\|\boldsymbol{x} - \boldsymbol{x}_\star\|)$, with $\alpha_1(\cdot), \alpha_2(\cdot), \alpha_3(\cdot) \in \mathcal{K}_\infty$.
- **A2.** $\mathbb{X}_0$ is viable, meaning that for each $\overline{\boldsymbol{x}} \in \mathbb{X}_0$, there exists $\overline{\boldsymbol{u}}_{\overline{\boldsymbol{x}}}$ such that

$$\boldsymbol{f}\left(\overline{\boldsymbol{x}}, \overline{\boldsymbol{u}}_{\overline{\boldsymbol{x}}}\right) \in \mathbb{X}_0. \tag{9}$$

- **A3.** For each $\overline{\boldsymbol{x}} \in \mathbb{X}_0$, there exists $\overline{\boldsymbol{u}}_{\overline{\boldsymbol{x}}}$ such that

$$V_N\left(\boldsymbol{f}\left(\overline{\boldsymbol{x}}, \overline{\boldsymbol{u}}_{\overline{\boldsymbol{x}}}\right)\right) + V\left(\overline{\boldsymbol{x}}, \overline{\boldsymbol{u}}_{\overline{\boldsymbol{x}}}\right) \leqslant V_N\left(\overline{\boldsymbol{x}}\right). \tag{10}$$

The proof of the theorem is given in [24] and it is omitted for brevity. Since the chosen cost function $V\left(\widehat{\boldsymbol{x}}(j), \overline{\boldsymbol{u}}(j)\right)$ in (7) is a sum of quadratic forms with positive definite matrices, it is straightforward to verify the first part of **A1**. It remains to construct the terminal cost V_N and the terminal inequality constraint through $\mathbb{X}_0$ such as the assumptions in Theorem 1 are satisfied. Following [24], a linear quadratic regulator (LQR) is employed to get a penalty matrix $\boldsymbol{P} \in \mathbb{R}^{2\times 2}$.

Then, V_N and $\mathbb{X}_0$ are constructed from $\boldsymbol{P}$. The following procedure is carried out at each time step k before solving (7).
Step 1 Locally linearize the dynamic system (8) at the references $\boldsymbol{x}_\star$ and $\boldsymbol{u}_\star$ as

$$\widetilde{\boldsymbol{f}}(\overline{\boldsymbol{x}}, \overline{\boldsymbol{u}}) = \boldsymbol{A}\overline{\boldsymbol{x}} + \boldsymbol{B}\overline{\boldsymbol{u}}, \tag{11}$$

with $\boldsymbol{A} = \frac{\partial \boldsymbol{f}(\overline{\boldsymbol{x}}, \overline{\boldsymbol{u}})}{\overline{\boldsymbol{x}}}\Big|_{(\boldsymbol{x}_*, \boldsymbol{u}_*)}$ and $\boldsymbol{B} = \frac{\partial \boldsymbol{f}(\overline{\boldsymbol{x}}, \overline{\boldsymbol{u}})}{\overline{\boldsymbol{u}}}\Big|_{(\boldsymbol{x}_*, \boldsymbol{u}_*)}$.
Step 2 Solve the following discrete-time algebraic Riccati equation and get the penalty matrix $\boldsymbol{P}$, which is positive definite and symmetric

$$\boldsymbol{P} = \boldsymbol{A}^T\boldsymbol{P}\boldsymbol{A} - \left(\boldsymbol{A}^T\boldsymbol{P}\boldsymbol{B}\right)\left(\boldsymbol{R} + \boldsymbol{B}^T\boldsymbol{P}\boldsymbol{B}\right)^{-1}\left(\boldsymbol{B}^T\boldsymbol{P}\boldsymbol{A}\right) + \boldsymbol{Q}. \tag{12}$$

Step 3 Design a control law $\overline{\boldsymbol{u}}_{\overline{\boldsymbol{x}}}$, meeting (9) and (10), as the feedback law for the LQR problem applied to the linearized system (11)

$$\overline{\boldsymbol{u}}_{\overline{\boldsymbol{x}}} = -\left(\boldsymbol{R} + \boldsymbol{B}^T\boldsymbol{P}\boldsymbol{B}\right)^{-1}\boldsymbol{B}^T\boldsymbol{P}\boldsymbol{A}\overline{\boldsymbol{x}}. \tag{13}$$

Step 4 Let $\sigma \in \mathbb{R}^+$ and $\delta \in \mathbb{R}^+$ be two constants. Assume $\hat{V} = (\boldsymbol{x}^\star - \overline{\boldsymbol{x}})^T\boldsymbol{P}(\boldsymbol{x}^\star - \overline{\boldsymbol{x}})$ and compute $\mathbb{X}_0$ and $V_N(\overline{\boldsymbol{x}})$ as

$$\begin{cases} V_N(\overline{\boldsymbol{x}}) := \sigma\hat{V}(\overline{\boldsymbol{x}}) \\ \mathbb{X}_0 := \{\overline{\boldsymbol{x}} |\ \hat{V}(\overline{\boldsymbol{x}}) \in \mathbb{R}^2 \leqslant \delta\} \end{cases} \tag{14}$$

Remark It is worth highlighting that the control law $\overline{\boldsymbol{u}}_{\overline{\boldsymbol{x}}}$ is only needed to compute $V_N(\overline{\boldsymbol{x}})$ and $\mathbb{X}_0$ at each sampling time k, and it is not applied to the real system. Once $V_N(\overline{\boldsymbol{x}})$ and $\mathbb{X}_0$ are obtained, the NLP (7) is solved to address the NPMC algorithm. Then, at each sampling time k, folding (14) into (7) and solving (7), the optimal control sequence $\overline{\boldsymbol{u}}^*(0)$, $\overline{\boldsymbol{u}}^*(1), \ldots, \overline{\boldsymbol{u}}^*(N-1)$ is obtained. Defining the NMPC feedback law $\boldsymbol{u}(k) := \overline{\boldsymbol{u}}^*(0)$, the system state at sampling time $k+1$ is obtained. In this way, the asymptotic stability of the closed-loop system $\boldsymbol{x}(k+1) = \boldsymbol{f}(\boldsymbol{x}(k), \boldsymbol{u}(k))$ with NMPC feedback law $\boldsymbol{u}(k)$ is guaranteed.

V. CASE STUDIES

Two case studies are developed in this section to validate the proposed NMPC and test its robustness. Within the technical report, the first preliminary experiment on a prototype without propellers is shown. The former case study includes white noise on the measurements, parametric uncertainty on the mass of the vehicle, a one-step delay in the controller. The latter case study considers a different physics engine to simulate the system dynamics. The model parameters of the WUAV are retrieved from the first prototypes under development within HYFLIERS, while the specifications on the parameters of the pipe are given from the oil and gas facilities involved in the project. The parameters employed in these case studies are thus selected as $m = 5$ kg, $L = 0.15$ m, $R_w = 0.02$ m, $\gamma_s = \pi/3$, $\theta_s = \pi/6$, $\mu = 0.85$, $R_p = 4$ in $\simeq 0.1016$ m. Besides, the control inputs must lie within the following bounds $-10 \leq u_1 < 10$ N and $-200 \leq u_2, u_3 \leq 200$ N·m. The state space is instead limited by $\mathbb{X} := \{\boldsymbol{x} \in \mathbb{R}^2 : -20 \leq x_1 \leq 20 \text{ deg},\ x_2 \in \mathbb{R}\}$.

A. Case 1: Numerical test

The numerical tests are performed on a standard PC through the MATLAB/SIMULINK software environment under the R2018a distribution. The real dynamic system (3) is numerically simulated through the $ode45$ solver with a maximum time step which is ten times lower the T_s employed to run the discrete-time optimal control problem (7). A first-order filter with a time constant of 0.2 s is implemented for u_1 before applying it to the real system (3) to simulate the slower propellers dynamics of the WUAV compared to the wheels. All the presented simulations have a duration of 8 s.

The robustness of the designed NMPC controller is tested by considering a white noise, whose standard deviation is $3.16 \cdot 10^{-4}$, on the measurements of $\boldsymbol{x}$ from the simulated real system; a one-step time-delay of the controller; a parametric uncertainty about the mass of the WUAV, in particular, the mass considered by the controller is 5.5 kg (10 % more of the value employed to simulate the real system). The sampling time is $T_s = 0.01$ s. The gains of the NLP have been practically tuned by a trial and error procedure. The values employed within numerical tests are $\boldsymbol{Q}$=diag$\{0.5, 0.04\}$ and $\boldsymbol{R}$=diag$\{0.04, 0.4, 0.4\}$. The matrices to compute V_N and $\mathbb{X}_0$ are given by $\boldsymbol{A} = \begin{bmatrix} 0 & 1; 65.4 & 0 \end{bmatrix}$ and $\boldsymbol{B} = \begin{bmatrix} 0 & 0 & 0; 1.2121 & 52.4864 & 52.4864 \end{bmatrix}$. By solving the discrete-time algebraic Riccati equation (11), the penalty matrix is $\boldsymbol{P} = \text{diag}\{0.8097, 0.8497\}$. The gains in (14) are thus tuned as $\sigma = 1.1$ and $\delta = 0.15$.

The objective is twofold: first, the investigation of how N affects the control design; then, through a reasonable value of N, different initial positions of the WUAV are considered.

1) Numerical simulations for different time horizons: The initial position of WUAV is chosen as $\theta = x_1 = 20$ deg, meaning that the device is subject to about 35% of the gravity acceleration. The prediction horizon N is selected as 6, 8, 10, and 12, respectively. The computational time in MATLAB is 138 s, 212 s, 300 s, and 418 s, respectively. Notice that these values can be reduced by employing optimized libraries written in low-level compiled languages (e.g., C, C++, ...). The obtained simulations are depicted in Fig. 4. The oscillatory behaviour is mostly due to the added delays and uncertainties. The following legend is useful to understand the different sub-figures: (a) and (b) correspond to the time histories of the angular position θ and the angular velocity $\dot{\theta}$ of the WUAV on the pipe, respectively; (c) shows the fulfilment of the constraints (4) and (6), in particular $FNi := \boldsymbol{F_s}^T\boldsymbol{n_i}\,(i = 1)$, $FNi := |\boldsymbol{F_s}^T\boldsymbol{t_0}| - \mu_0\boldsymbol{F_s}^T\boldsymbol{n_0}\,(i = 2)$, $FNi := |\tau_{w1}| - \frac{\mu m g R_w cos(\theta)}{2cos(\theta_s)}\,(i = 3)$, and $FNi := |\tau_{w2}| - \frac{\mu m g R_w cos(\theta)}{2cos(\theta_s)}\,(i = 4)$; (d-f) depict the control inputs. In particular, Fig. 4(c) shows only the case $N = 6$.

In the numerical simulation, the stabilization constraints (4) and (6) are fulfilled, while the curves are not as smooth due to the disturbance on the controller. Besides, the control inputs $\boldsymbol{u}$ does not tend to zero with small N. Within Fig. 4, when $N = 6$, the input $\boldsymbol{u}$ tends to $\begin{bmatrix} -0.03 & 0 & 0 \end{bmatrix}^T$, which is worse than the tendency of $\boldsymbol{u} = \begin{bmatrix} -0.006 & 0 & 0 \end{bmatrix}^T$ when $N = 8$ and

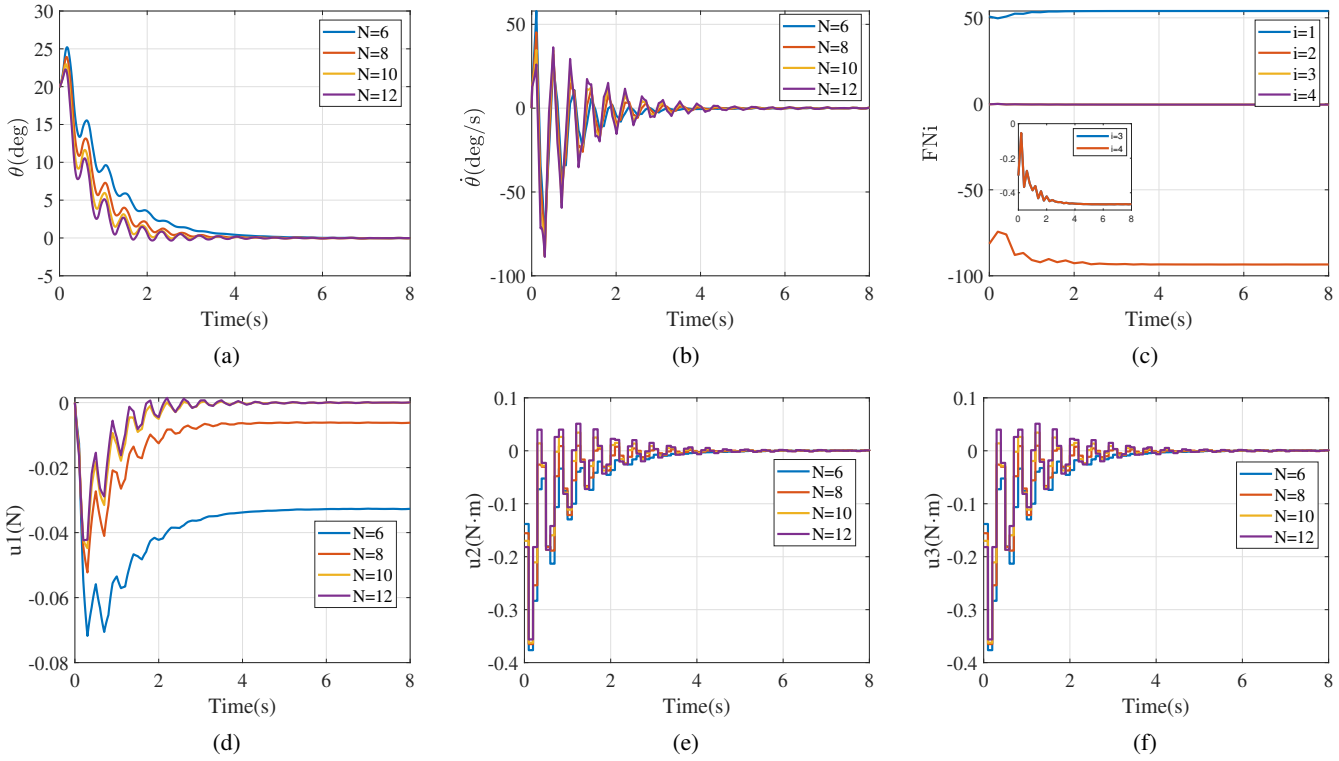

Fig. 4. Case study 1: numerical test. Numerical simulations for different time horizons. (a)-Time history of θ. (b)-Time history of $\dot{\theta}$. (c)-Time histories to check the fulfilment of the constraints (4) and (6). (d)-(f) Time histories of the control inputs.

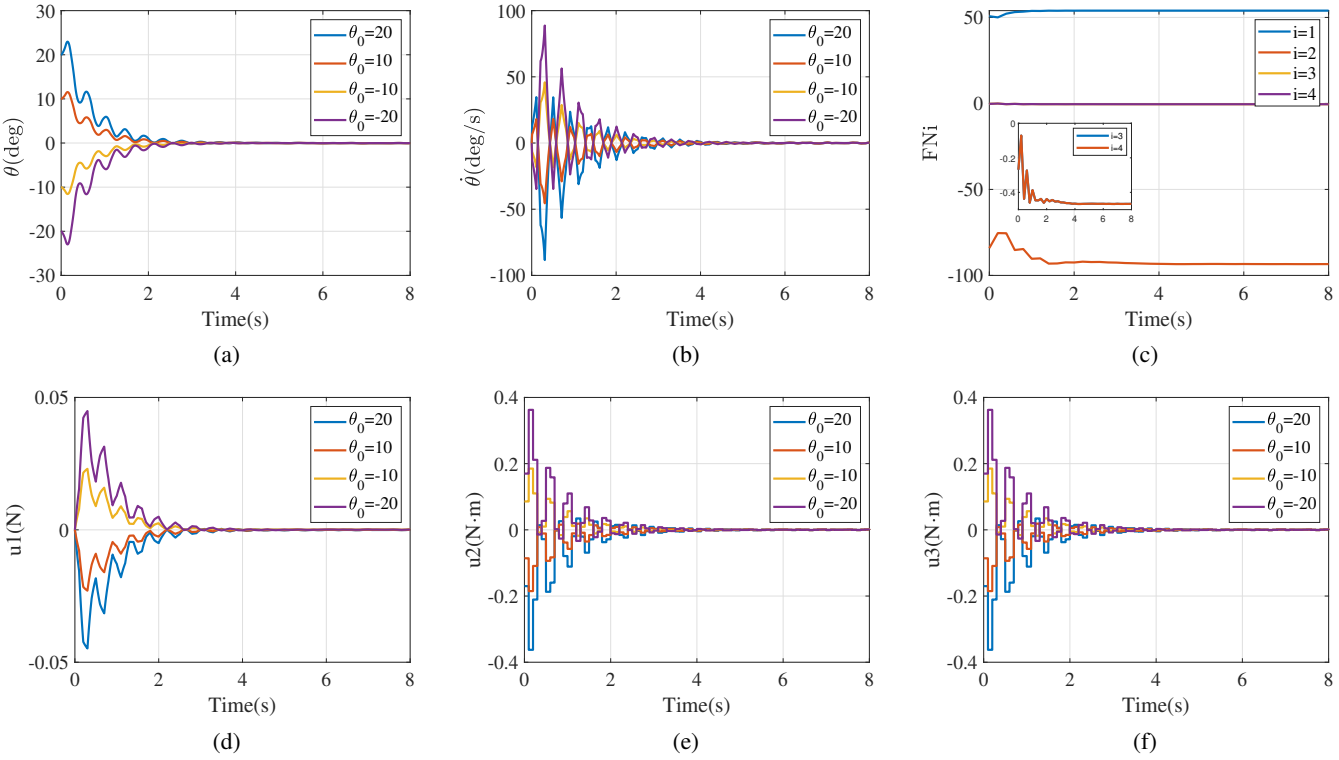

Fig. 5. Case study 1: numerical test. Numerical simulations for different initial conditions. (a)-Time history of θ. (b)-Time history of $\dot{\theta}$. (c)-Time histories to check the fulfilment of the constraints (4) and (6). (d)-(f) Time histories of the control inputs.

the tendency of $\boldsymbol{u} = \begin{bmatrix} -6e^{-5} & 0 & 0 \end{bmatrix}^T$ when $N = 10$ and $N = 12$.

By observing the behaviour of the time histories and the above analysis, together with the fact that large N increases

the computational effort, it may be worth selecting $N = 10$.

2) Numerical simulations for different initial conditions: From the predefined $T_s = 0.01$ s and the selected $N = 10$, different initial values of the WUAV on the pipe are tackled in this cases study. In particular, the considered initial values for θ are ± 20 deg and ± 10 deg, since they contribute to the high visibility of the generated figure and the related symmetry of the plots. The obtained time histories are represented in Fig. 5, with the legend mentioned above. Fig. 5(c) represent the case with initial value of 20 deg. The plots show that the controller can stabilize the WUAV on the pipe from any of the considered initial condition, while the control inputs remain within the considered bounds, and the other constraints are fulfilled.

B. Case 2: Dynamic simulation

In this second case study, a dynamic simulation is carried out by using the V-REP simulator and MATLAB. The former is not employed as a visualizer of the simulation, but its physics engine simulates the system dynamics. The latter implements the proposed NMPC algorithm, and it is connected with V-REP through suitable remote application programming interfaces. A video of the simulation is available as a multimedia attachment.

A proper time synchronization has been ensured using the synchronous modality provided inside V-REP, with the control loop running at 25 ms. In V-REP the simulated system is dynamically enabled considering physically consistent dynamic parameters for the rover mass and inertia and the wheel-pipe friction. In particular, the following parameters change from the first case study because they are given by the CAD model in Fig. 2 that has been imported into V-REP: $m = 6.1$ kg, $\mu = 0.8$, $L = 0.11$ m, $R_w = 0.02$ m, $\gamma_s = 70.6$ deg, $\theta_s = \pi/4$ rad. The wheels are actuated with a torque controller applied on the simulated joint motors. The V-REP model of Fig. 2 is not planar, but it is symmetric to the vertical plane cutting the WUAV at its center of mass. Therefore, the torques of the wheels obtained from the NMPC algorithm running in MATLAB are equally split between each of the symmetric pair of wheels in V-REP. On the other hand, a force has been applied to the rover to simulate the propeller lift force. The gains of the NLP have been practically tuned by a trial and error procedure. The values employed within such a dynamic simulation are $\boldsymbol{Q}$=diag$\{0.5, 0.3\}$ and $\boldsymbol{R}$=diag$\{0.01, 0.4, 0.4\}$. The control horizon is set to $N = 7$. The presented simulations has a duration of 28 s. Other parameters are left unchanged.

The obtained simulations are depicted in Fig. 6, with the legend mentioned above. The initial condition is set to -20 deg with initial control input equal to zero. For this reason, it is possible to appreciate a peak at the initial time instant in the control inputs depicted in Fig. 6(d)-(f), and in the resulting velocity shown in Fig. 6(b). The plots show that the controller can stabilize the WUAV on the pipe also during the carried out dynamic simulation (see Fig. 6(a)). Besides, the control inputs remain within the considered bounds, and the other constraints are fulfilled (see Fig. 6(c)). The behaviour is less smooth than the previous case study since the physics engine of V-REP does not rely on the system modelled through (3), and it does not take into account all the assumptions made at the beginning of Section III. This is a further demonstration of the robustness performance of the designed control algorithm.

VI. CONCLUSION

This letter addressed the problem of stabilizing a WUAV on a pipe. The Newton-Euler dynamic equation of the system was derived, along with some constraints necessary to stabilize the WUAV on the pipe. The asymptotic stability of the designed NMPC was guaranteed from proper terminal cost and inequality constraints derived through an LQR approach. Numerical tests and dynamic simulation were presented to bolster the efficiency of the method, even in the presence of band-limited disturbances, time-delays, parametric uncertainties, and a different physics engine to simulate the systems dynamics. Current work is focused on practical implementation. Preliminary results, not yet mature to be presented here, are present in the technical report and the video attached as multimedia material.

REFERENCES

[1] T. Bartelds, A. Capra, S. Hamaza, S. Stramigioli, and M. Fumagalli, "Compliant aerial manipulators: Toward a new generation of aerial robotic workers," *IEEE Robotics and Automation Letters*, vol. 1, no. 1, pp. 477–483, 2016.

[2] H. Wopereis, T. van der Molen, T. Post, S. Stramigioli, and M. Fumagalli, "Mechanism for perching on smooth surfaces using aerial impacts," in *2016 IEEE International Symposium on Safety, Security, and Rescue Robotics*, Lausanne, Switzerland, 2016, pp. 154–159.

[3] H. Wopereis, J. Hoekstra, T. Post, G. Folkertsma, S. Stramigioli, and M. Fumagalli, "Application of substantial and sustained force to vertical surfaces using a quadrotor," in *2017 IEEE International Conference on Robotics and Automation*, Singapore, 2017, pp. 2704–2709.

[4] A. Suarez, P. Sanchez-Cuevas, M. Fernandez, G. Perez, M. Heredia, and A. Ollero, "Lightweight and compliant long reach aerial manipulator for inspection operations," in *2018 IEEE/RSJ International Conference on Intelligent Robots and Systems*, Madrid, Spain, 2018, pp. 6746–6752.

[5] D. Schmidt and K. Berns, "Climbing robots for maintenance and inspections of vertical structures a survey of design aspects and technologies," *Robotics and Autonomous Systems*, vol. 61, no. 12, pp. 1288–1305, 2013.

[6] W. R. Roderick, M. R. Cutkosky, and L. D., "Touchdown to take-off: at the interface of flight and surface locomotion," *Interface Focus*, vol. 7, no. 1, pp. 1–15, 2017.

[7] M. Tavakoli, L. Marques, and A. T. de Almeida, "Omniclimber: An omnidirectional light weight climbing robot with flexibility to adapt to non-flat surfaces," in *IEEE/RSJ International Conference on Intelligent Robots and Systems*, Vilamoura, Portugal, 2012, pp. 280–285.

[8] Y. Yoshida and S. Ma, "Design of a wall-climbing robot with passive suction cups," in *IEEE International Conference on Robotics and Biomimetics*, Tianjin, China, 2010, pp. 1513–1518.

[9] W. Chi, K. H. Low, K. H. Hoon, and J. Tang, "An optimized perching mechanism for autonomous perching with a quadrotor," in *IEEE International Conference on Robotics and Automation (ICRA)*, Hong Kong, China, 2014, pp. 3109–3115.

[10] M. A. Graule, P. Chirarattananon, S. B. Fuller, N. T. Jafferis, K. Y. Ma, M. Spenko, R. Kornbluh, and R. J. Wood, "Perching and takeoff of a robotic insect on overhangs using switchable electrostatic adhesion," *Science*, vol. 352, no. 6288, pp. 978–982, 2016.

[11] N. Wiltsie, M. Lanzetta, and K. Iagnemma, "A controllably adhesive climbing robot using magnetorheological fluid," in *IEEE International Conference on Technologies for Practical Robot Applications (TePRA)*, MA, USA, 2012, pp. 91–96.

[12] A. Baghani, M. Ahmadabadi, and A. Harati, "Kinematics modeling of a wheel-based pole climbing robot (UT-PCR)," in *2005 IEEE International Conference on Robotics and Automation*, Barcelona, Spain, 2005, pp. 2099–2104.

[13] G. Haynes, A. Khripin, G. Lynch, J. Amory, A. Saunders, A. Rizzi, and D. Koditschek, "Rapid pole climbing with a quadrupedal robot," in *2009 IEEE International Conference on Robotics and Automation*, Kobe, Japan, 2009, pp. 2767–2772.

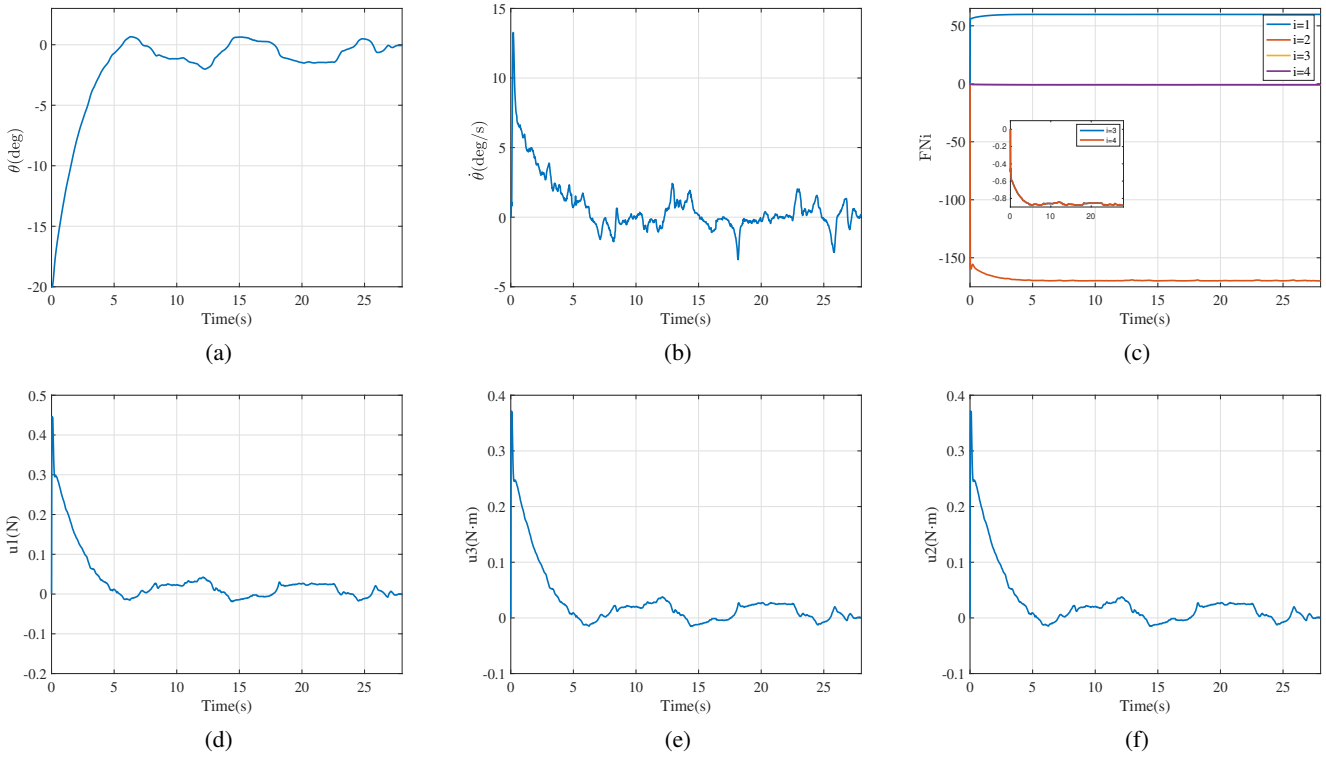

Fig. 6. Case study 2: dynamic simulation. (a)-Time history of θ. (b)-Time history of $\dot{\theta}$. (c)-Time histories to check the fulfilment of the constraints (4) and (6). (d)-(f) Time histories of the control inputs.

[14] Y. Song, C. Lee, I. Koo, D. Tran, H. Moon, and H. Choi, "Development of wall climbing robotic system for inspection purpose," in *2008 IEEE/RSJ International Conference on Intelligent Robots and Systems*, Nice, France, 2008, pp. 1990–1995.

[15] M. Spenko, G. Haynes, J. Saunders, M. Cutkosky, A. Rizzi, and D. Koditschek, "Biologically inspired climbing with a hexapedal robot," *Journal of Field Robotics*, vol. 25, no. 4, pp. 223–242, 2008.

[16] W. Fischer, F. Tache, and R. Siegwart, "Inspection system for very thin and fragile surfaces, based on a pair of wall climbing robots with magnetic wheels," in *2007 IEEE/RSJ International Conference on Intelligent Robots and Systems*, San Diego, CA, USA, 2007, pp. 1216–1221.

[17] G. J., M. Prieto, M. Armada, and P. Gonzalez de Santos, "A six-legged climbing robot for high payloads," in *International Conference on Control Applications*, Trieste, Italy, 1998, pp. 446–450.

[18] B. Kocer, T. Tjahjowidodo, and G. Lee, "Constrained estimation–based nonlinear model predictive control for UAV-elastic tool interaction," in *2018 IEEE/ASME International Conference on Advanced Intelligent Mechatronics*, Auckland, New Zeland, 2018, pp. 466–471.

[19] S. Qin and T. Badgwell, "A survey of industrial model predictive control technology," *Control Engineering Practice*, vol. 11, no. 7, pp. 733–764, 2003.

[20] K. Aström and T. Hägglund, "The future of PID control," *Control Engineering Practice*, vol. 9, no. 11, pp. 1163–1175, 2001.

[21] F. Salem and M. Mosaad, "A comparison between MPC and optimal PID controllers: Case studies," in *Michael Faraday IET International Summit 2015*, Kolkata, India, 2015, pp. 59–65.

[22] S. Li and Y. Zheng, *Distributed model predictive control for plant-wide systems*. Wiley, 2015.

[23] F. A. Fontes, "A general framework to design stabilizing nonlinear model predictive controllers," *Systems & Control Letters*, vol. 42, no. 2, pp. 127–143, 2001.

[24] L. Grüne and J. Pannek, *Nonlinear model predictive control: theory and algorithms, communications and control engineering*. Springer International publishing Switzerland, 2017.

[25] H. Michalska and D. Q. Mayne, "Robust receding horizon control of constrained nonlinear systems," *IEEE Transactions on Automatic Control*, vol. 38, no. 11, pp. 1623–1633, 1993.

[26] G. De Nicolao, L. Magni, and R. Scattolini, "Stabilizing receding-horizon control of nonlinear time-varying systems," *IEEE Transactions on Automatic Control*, vol. 43, no. 7, pp. 1030–1036, 1998.

[27] L. Magni, G. De Nicolao, L. Magnani, and R. Scattolini, "A stabilizing model-based predictive control algorithm for nonlinear systems," *Automatica*, vol. 37, no. 9, pp. 1351–1362, 2001.

[28] J. S. Mejia and D. M. Stipanovic, "Asymptotic stabilization using a constructive approach to constrained nonlinear model predictive control," in *47th IEEE Conference on Decision and Control*, Cancun, Mexico, 2008, pp. 4061–4066.

[29] R. Gao, J. Xu, and H. Zhan, "Receding horizon control for multiplicative noise stochastic systems with input delay," *Automatica*, vol. 81, pp. 390–396, 2017.

[30] D. F. He, H. Huang, and Q. X. Chen, "Stabilizing model predictive control of time-varying non-linear systems using linear matrix inequalities," *IMA Journal of Mathematical Control and Information*, vol. 33, no. 1, pp. 21–35, 2014.

[31] V. Duindam and S. Stramigioli, *Modeling and control for efficient bipedal walking robots. A port-based approach*, ser. Springer Tracts in Advanced Robotics, B. Siciliano, O. Khatib, and F. Groes, Eds. Springer-Verlag Berlin Heidelberg, 2009, vol. 53.

[32] V. L. Popov, *Contact mechanics and friction*. Springer Berlin Heidelberg, 2010.

[33] S. Konduri, E. Orlando, C. Torres, and P. Pagilla, "Effect of wheel slip in the coordination of wheeled mobile robots," in *19th World Congress*, Cape Town, South Africa, 2014, pp. 8097–8102.